coatings

MDPI

Article

Hydrothermal Synthesis of Cobalt Ruthenium Sulfides as Promising Pseudocapacitor Electrode Materials

Ravi Bolagam [1] and Sukkee Um [1,*]

Department of Mechanical Engineering, Hanyang University, 222 Wangsimni-ro, Seongdong-gu, Seoul 04763, Korea; bolgam.ravi@gmail.com

* Correspondence: sukkeeum@hanyang.ac.kr; Tel./Fax: +82-2-2220-0432

Received: 14 January 2020; Accepted: 21 February 2020; Published: 25 February 2020

Abstract: In this paper, we report the successful synthesis of cobalt ruthenium sulfides by a facile hydrothermal method. The structural aspects of the as-prepared cobalt ruthenium sulfides were characterized using X-ray diffraction, X-ray photoelectron spectroscopy, and Raman spectroscopy. All the prepared materials exhibited nanocrystal morphology. The electrochemical performance of the ternary metal sulfides was investigated by cyclic voltammetry (CV), galvanostatic charge-discharge (GCD), and electrochemical impedance spectroscopy techniques. Noticeably, the optimized ternary metal sulfide electrode exhibited good specific capacitances of 95 F g^{-1} at 5 mV s^{-1} and 75 F g^{-1} at 1 A g^{-1}, excellent rate capability (48 F g^{-1} at 5 A g^{-1}), and superior cycling stability (81% capacitance retention after 1000 cycles). Moreover, this electrode demonstrated energy densities of 10.5 and 6.7 Wh kg^{-1} at power densities of 600 and 3001.5 W kg^{-1}, respectively. These attractive properties endow proposed electrodes with significant potential for high-performance energy storage devices.

Keywords: cobalt ruthenium sulfide; supercapacitor; hydrothermal method; ternary metal sulfides; electrochemical impedance spectrum

1. Introduction

Supercapacitors (SCs) or ultracapacitors, also known as electrochemical capacitors, have attracted intense attention as a principal class of clean and sustainable energy storage devices for modern electronics because of their impressive energy storage potential, with excellent electrochemical reversibility, long lifespan, ultrahigh power density, quick charge/discharge capability, strong safety record, and environmental friendliness. Due to these advantages, SCs hold great promise for next generation energy storage applications, such as regenerative braking for automobiles, uninterruptible power supply systems, and portable electronics [1–3].

In general, supercapacitors can be categorized into pseudocapacitors (redox supercapacitors) and electrochemical double layer capacitors (EDLCs) based on their charge storage mechanism and active materials [2–4]. The electrochemical performance of SCs mainly depends on the properties of the active electrode materials; these should possess good electronic conductivity, large specific surface area, high chemical stability, nanoscale topography, and redox chemistry [4–6]. To date, carbon electrodes in EDLCs and metal oxides/hydroxides and conducting polymers in pseudocapacitors have been broadly exploited as promising electrode materials. Carbon based supercapacitors store energy through adsorption/desorption of ions at the double layer interface between the active electrode and the electrolyte [7]. Metal oxides/hydroxides (RuO_2, Co_3O_4, MnO_2, NiO, TiO_2, $Co(OH)_2$, etc.) [8–12] and conducting polymers (polyaniline, polypyrrole, polythiophene, etc.) [13–15] show much greater specific capacitances than carbon materials by virtue of their rich reversible Faradaic redox reactions,

which occur between the electrode material and the electrolyte [16,17]. Carbon materials show lower energy densities and superior cycle stabilities compared to pseudocapacitive materials [18,19]. On the other hand, metal oxides/hydroxides are hampered by their low electrical conductivity and rate capability; and conducting polymers, by their poor cycling stability. These disadvantages currently prevent their use in a wide range of commercial applications [20,21]. So, from a practical point of view, there is an urgent need to develop supercapacitors with high energy density without sacrificing cycle life or rate capability. The key to addressing these challenges is the design and development of advanced electrode materials.

Recently, in the pseudocapacitive materials category, transition metal chalcogenides have gained much interest as potential electrode materials in energy storage applications because of their higher electrical conductivity and multiple available oxidation states, promoting rapid redox reactions compared to their metal oxide or hydroxide counterparts [22–24]. Transition metal sulfides, including cobalt sulfides, nickel sulfides, copper sulfides, ruthenium sulfides, iron sulfides, and molybdenum sulfides, have been employed as electrode materials for energy storage applications [25–28]. Sulfur ions tend to produce flexible nanostructures because of their high electroconductivity and fast charge transport [29]. Amongst these, cobalt sulfide (CoS_x), with its various stoichiometric compositions, such as Co_9S_8, Co_3S_4, CoS_2, and CoS, has been gaining tremendous interest owing to its intriguing physical and chemical properties [30,31]. Ruthenium based materials have also been proven to be the best electrodes for energy storage applications by virtue of their excellent electrochemical properties [29,32,33].

The chemical composition and associated redox properties are factors of primary importance for energy-storage materials. Additionally, many factors affect the rate performance of electrodes, including the morphology, surface properties, microstructure, conductivity, and components of the electrode materials. Currently, ternary metal sulfides have been proposed to overcome some issues with single component metal sulfides or ternary metal oxides, such as rate capability and cycle life [34]. The combination of two different metals can enhance the redox chemistry of the materials and their performance in electrochemical systems when compared with single-metal sulfides. A new ruthenium cobalt oxide ($RuCo_2O_4$) material has been prepared by a simple electrodeposition method and demonstrated as an advanced electrode material for supercapacitors [35]. Ternary metal sulfides like $NiCo_2S_4$, $CuCo_2S_4$, and $MnCo_2S_4$ possess much higher electrochemical activity and capacity due to their multiple oxidation states and smaller band gaps, thus allowing for rich redox reactions [36,37]. However, it is still unclear if these materials exhibit any enhancement in electronic conductivity and capacitance as a result.

Metal sulfides have been employed as potential electrode materials in various applications such as batteries, supercapacitors, electro−catalysts, and solar cells [38–42]. Furthermore, various ternary transition metal sulfides have already been studied as efficient electrode materials for supercapacitors [37,43–45]. Particularly, $NiCo_2S_4$ has been studied most comprehensively [46–48]. Although ternary metal sulfides have been studied as potential electrode materials for energy storage applications, metal sulfides normally exhibit low rate capability and cycle life stability. To overcome these drawbacks, there is an urgent need to design electrode architectures with good electronic conductivity, plentiful electron transport channels, and robust structural stability [49].

Inspired by the research summarized above, we studied the electrochemical performance of cobalt ruthenium sulfides as advanced electrode materials for supercapacitor applications. The improved electrochemical performance of ternary metal sulfides in terms of energy density, rate capability, and cycling stability from the combination of the two different metal components can enhance the redox chemistry of the materials by efficient synergetic effects. Herein, we report a simple hydrothermal strategy that was employed to prepare cobalt ruthenium sulfides using aqueous solutions of $CoCl_2{\cdot}6H_2O$ and $RuCl_3{\cdot}nH_2O$ as metal sources and thioacetamide as a sulfur source.

We investigated the electrochemical performance of cobalt ruthenium sulfides synthesized with different molar ratios and different reaction times in a 0.5 M H_2SO_4 aqueous electrolyte using a

three-electrode configuration. A series of electrochemical measurements were conducted, including cyclic voltammetry (CV) at various scan rates, galvanostatic charge-discharge (GCD) cycling at various applied currents, and electrochemical impedance spectroscopy (EIS) at the open circuit voltage. The effect of reaction time on the electrochemical performance and microstructure of the cobalt ruthenium sulfides was investigated.

2. Materials and methods

2.1. Materials

Cobalt (II) chloride hexahydrate ($CoCl_2 \cdot 6H_2O$) and thioacetamide were purchased from Samchun Pure Chemicals (Seoul, Korea). Ruthenium (III) chloride hydrate ($RuCl_3 \cdot nH_2O$) was purchased from Kojima Chemicals (Toyota-shi, Japan), and polyvinylpyrrolidone (PVP) was purchased from Alfa Aesar, Ward Hill, MA, USA.

2.2. Material Synthesis

Preparation of Cobalt Ruthenium Sulfide Materials

In a typical experiment, 2 mmol of cobalt (II) chloride hexahydrate (475.9 mg), 1 mmol of ruthenium (III) chloride hydrate (207.4 mg), and 8 mmol of thioacetamide (601 mg), PVP (70 mg) were dissolved in 80 mL of H_2O. After stirring for 1 h, the solution was transferred into a 100 mL Teflon-lined stainless-steel autoclave and kept at 160 °C for 24 h. After cooling, the precipitate was vacuum filtered, washed several times with deionized water and ethanol, and then dried at 50 °C for 12 h. The precursor mixture was heat-treated at 650 °C for 2 h under a N_2 atmosphere to produce crystalline cobalt ruthenium sulfides (Co_2RuS_6) as shown in Figure 1. This sample was denoted as Co_2RuS_6-24. The cobalt ruthenium sulfide samples were prepared through a similar process with different Co/Ru molar ratios of 1:2 and 1:1; these samples are denoted as $CoRu_2S_6$ and $CoRuS_6$, respectively. Similarly, cobalt ruthenium sulfide samples were prepared for 36 h and 48 h, denoted as Co_2RuS_6-36 and Co_2RuS_6-48, correspondingly. Pristine Co_9S_8 and RuS_2 were prepared following the above procedure in the absence of ruthenium chloride and cobalt chloride hexahydrate, respectively.

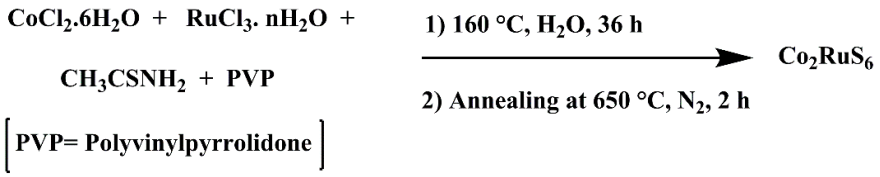

Figure 1. The representative chemical reaction for the synthesis of cobalt ruthenium sulfides.

2.3. Material Characterization

X-Ray photoelectron spectroscopy (XPS) was performed using a Theta Probe electron spectrometer (Thermo Fisher Scientific Co., Waltham, MA, USA). The crystallographic structures of the materials were determined using a Rigaku X-ray diffractometer (XRD; Rigaku, Tokyo, Japan) operated at 40 keV and 15 mA with a Cu Kα radiation source (λ = 1.54 Å). The chemical bonding transitions were analyzed by Fourier transform infrared spectroscopy (FT-IR; Thermo Scientific Nicolet 6700, Waltham, MA, USA) in the frequency range of 4000–400 cm^{-1} using KBr pellets. The morphologies were examined by high-resolution transmission electron microscopy (HR-TEM; JEOL JEM 2100F, Tokyo, Japan) and elemental analysis was conducted by energy-dispersive X-ray spectroscopy (EDS). Raman spectra of the composites were obtained using a Raman spectrometer (JASCO, NRS-3100, Tokyo, Japan) that was operated at 1.4 mW laser power with an excitation wavelength of 532 nm (green).

2.4. Electrode Preparation and Electrochemical Measurements

To prepare the working electrode, active materials were mixed with conductive carbon and polyvinylidene fluoride binder at a mass ratio of 80:10:10. For instance, first polyvinylidene fluoride (PVDF) (10 mg) dissolved in 1-methyl-2-pyrrolidinone (NMP) solvent to prepare solution. We have taken 80 mg active material, 10 mg carbon and grind in mortar for 30 min. Next add this grinded mixture into PVDF-NMP solution and stir for 24 h to obtain the electrode slurry. This slurry coated on stainless-steel substrate with brush in 1 cm × 1 cm area and dried in vacuum at 50 °C for overnight. Cyclic voltammetry (CV), galvanostatic charge/discharge (GCD), and electrochemical impedance spectroscopy (EIS) measurements were performed using a potentiostat/galvanostat (Gamry PGSTATZRA Reference 600, Warminster, PA, USA) in an aqueous 0.5 M H_2SO_4 electrolyte solution at room temperature using a standard three-electrode cell configuration. The working, counter, and reference electrodes were the active material-coated stainless-steel substrate, platinum wire, and an Ag/AgCl electrode, respectively. CV and GCD tests were carried out within the potential range of 0–1 V, while the EIS experiments were conducted in the frequency range from 100 kHz to 0.1 Hz at a 5.0mV amplitude relative to the open circuit potential.

3. Results and Discussion

During this synthesis procedure, the released metal ions (i.e., Co^{2+} and Ru^{3+}) react with sulfide (S^{2-}) ions from H_2S, which is generated by the hydrolytic reaction of thioacetamide due to the prolonged hydrothermal treatment, resulting in the formation of ternary metal sulfide nanoparticles. This method avoids the tedious multi-step hydrothermal treatment and solvothermal anion-exchange commonly used in previous studies [50]. In the literature, nickel sulfides and cobalt sulfides have also been prepared by using thioacetamide as sulfur source [51].

3.1. Characterization of Structure and Morphology

Figure 2a shows the powder X-ray diffraction (XRD) pattern of a Co_9S_8 sample heat treated at 650 °C in N_2 atmosphere. The characteristic diffraction peaks in Figure 2a, can be assigned to the (311), (222), (400), (331), (511), (440), (531), (622), (731), and (800) lattice planes of Co9S8 (JCPDS No. 19-0364). Major diffraction peaks could be readily indexed to Co9S8 crystallites with a face-centered cubic structure and a space group of *Fm-3m*(225) [52–54]. The broad and weak peaks may be caused by the poor crystallinity of the nanocrystals. Figure 2b shows the X-ray diffraction (XRD) pattern of an RuS_2 sample heat treated at 650 °C in N_2 atmosphere. The characteristic diffraction peaks of Figure 2b, can be indexed to the (111), (200), (210), (211), (222), (311), (220), (230), (321), (420), (421), (422), and (430) lattice planes of cubic phase RuS_2 (JCPDS No. 19-1107) with a space group of *Pa3*(205) [28,29]. Figure 2c,d are closely matched with Figure 2b. Figure 2e–g are very similar to Figure 2a. Further confirmation the chemical structures of cobalt ruthenium sulfides was obtained through FTIR, Raman, and XPS analyses.

To confirm the composition of the functional groups on the product obtained from the hydrothermal process followed by heat treatment at 650 °C in N_2 atmosphere for 2 h, we analyzed the FT-IR spectra of the samples at different time intervals. The FT-IR spectra of Co_2RuS_6-24 and Co_2RuS_6-36 are shown in Figure 3. The Co_2RuS_6-24 sample showed peaks at approximately 727, 533, 483, and 433 cm^{-1}, indicating S–S, Co–S, and Ru–S vibrational stretching modes, and peaks at 1607, 1415, 1283, 1006, and 833 cm^{-1} indicating C–O, Co–O, and Ru–O vibrational stretching modes [55]. The Co_2RuS_6-36 sample showed peaks at approximately 727, 556, 511, and 450 cm^{-1} indicating S–S, Co–S, and Ru–S vibrational stretching modes and peaks at 1614, 1417, 1285, 1012, and 833, cm^{-1} indicating C–O, Co–O, and Ru–O vibrational stretching modes [55].

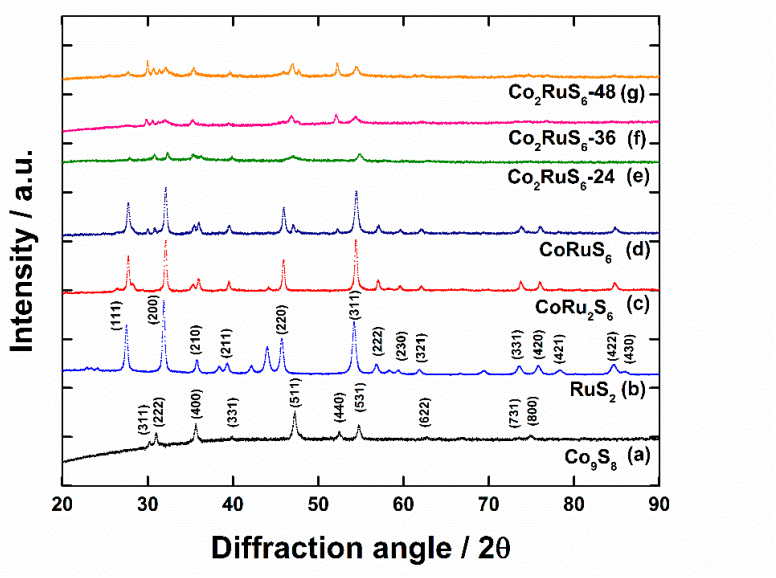

Figure 2. X-Ray diffraction patterns of (**a**) Co_9S_8, (**b**) RuS_2, (**c**) $CoRu_2S_6$, (**d**) $CoRuS_6$, (**e**) Co_2RuS_6-24, (**f**) Co_2RuS_6-36, and (**g**) Co_2RuS_6-48. All samples were heat-treated at 650 °C for 2 h in a N_2 atmosphere.

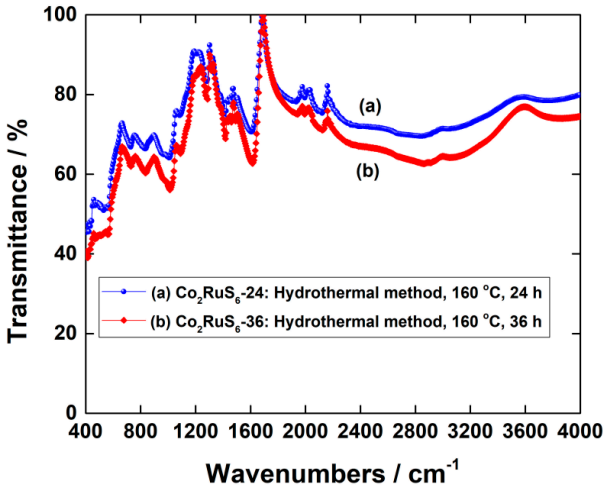

Figure 3. Fourier transform infrared spectra of (**a**) Co_2RuS_6-24, and (**b**) Co_2RuS_6-36.

In the Raman spectra shown in Figure 4, pristine RuS_2 showed characteristic peaks around 377 and 385 cm^{-1} which can be assigned to E_g and A_g modes, respectively [28]. Pristine Co_9S_8 showed characteristic peaks at approximately 662, 500, 475, and 188 cm^{-1} which correspond to the stretching S–S mode and the E_g mode of Co in cobalt sulfides [56]. Similarly, in cobalt ruthenium sulfides (Co_2RuS_6-24, 36, and 48), the characteristic peaks at 665, 505, 475, and 188 cm^{-1} are attributed to the stretching S-S mode and Eg mode of Co in cobalt ruthenium sulfides [57,58], and peaks at 375 (E_g) and 385 (A_g) cm^{-1} correspond to the stretching S–S mode of Ru in cobalt ruthenium sulfide bonds [28]. The above Raman spectra results indicate that the cobalt ruthenium sulfides (Co_2RuS_6) showed the characteristic modes of both cobalt sulfides and ruthenium sulfides.

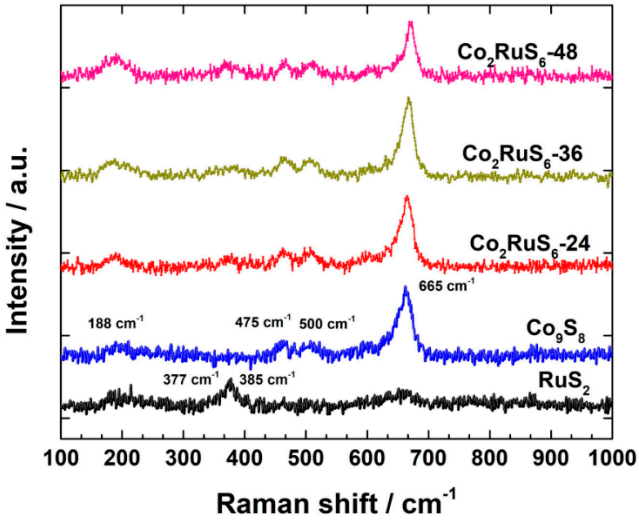

Figure 4. Raman spectra of RuS_2, Co_9S_8, Co_2RuS_6-24, Co_2RuS_6-36, and Co_2RuS_6-48.

Figure 5 shows HR-TEM images of the hydrothermally synthesized cobalt ruthenium sulfides. All cobalt ruthenium sulfide materials are irregular in shape, moderately polydisperse, and somewhat aggregated [59]. Figure 5a–c show nanocrystals with average sizes of 30, 50, and 20 nm, respectively. Figure 5d,e show nanocrystals approximately 50 nm in size. The pristine Co_9S_8 and RuS_2 particles shown in Figure 5f,g are approximately 20 and 15 nm in size, respectively. These morphology results reveal that in the preparation of Co_2RuS_6 ternary sulfides, when the reaction time is increased to 48 h, the resulting nanocrystal size decreases slightly. All cobalt ruthenium sulfides formed nanocrystals which were slightly larger than the nanocrystals of pristine RuS_2 and Co_9S_8. Similar to cobalt-iron-pyrites ($Co_{0.625}Fe_{0.375}S_2$) [60], the EDS spectrum confirms the coexistence of Co, Ru, and S elements in the Co_2RuS_6-36 material with an atomic ratio of 1.92:0.97:5.6 (Figure 6), which is in good agreement with the stoichiometry of Co_2RuS_6.

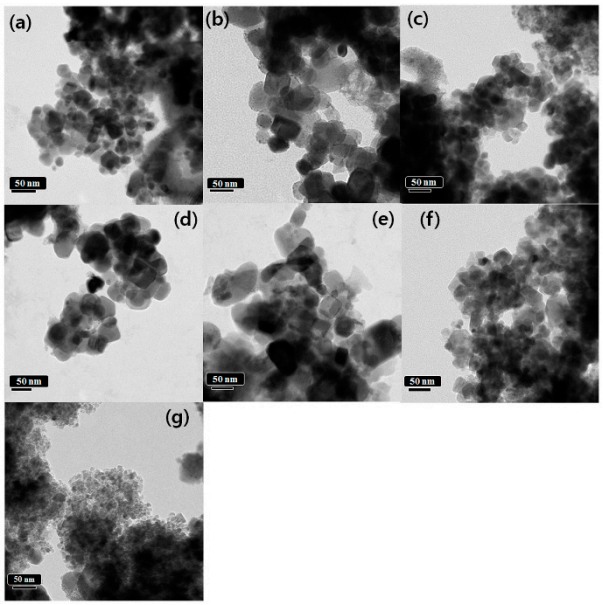

Figure 5. High-resolution transmission electron micrographs of (**a**) Co_2RuS_6-24, (**b**) Co_2RuS_6-36, (**c**) Co_2RuS_6-48, (**d**) $CoRu_2S_6$, (**e**) $CoRuS_6$, (**f**) Co_9S_8, and (**g**) RuS_2. All samples were heat-treated at 650 °C for 2 h in a N_2 atmosphere.

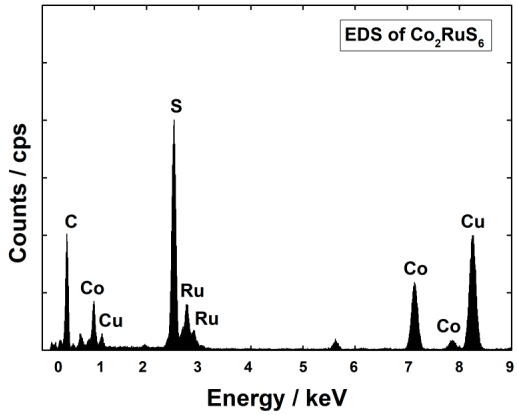

Figure 6. EDS pattern of the Co_2RuS_6-36 sample after annealing at 650 °C in N_2.

To further characterize the elemental chemical composition and detailed bonding configurations of the samples, XPS measurements were carried out, and Figure 7 demonstrates that the as-prepared samples are mainly composed of Co, Ru, and S elements without any obvious impurities (O peaks originate from surface oxidation of materials). The XPS survey spectra of the cobalt ruthenium sulfides (Figure 7a) confirmed the presence of Co 2*p*, Ru 3*d*, Ru 3*p*, S 2*p*, and O 1*s* states. As shown in Figure 7b, two prominent peaks were observed at binding energies of 778.2 and 793.4 eV corresponding to the Co $2p_{3/2}$ and Co $2p_{1/2}$ spin–orbit peaks, respectively, which confirmed the existence of two kinds of cobalt oxidation states: Co^{2+} and Co^{3+} [49,61]. The spin–orbit splitting of Co $2p_{1/2}$ and Co $2p_{3/2}$ is over 15 eV, suggesting the coexistence of Co^{2+} and Co^{3+} [62].

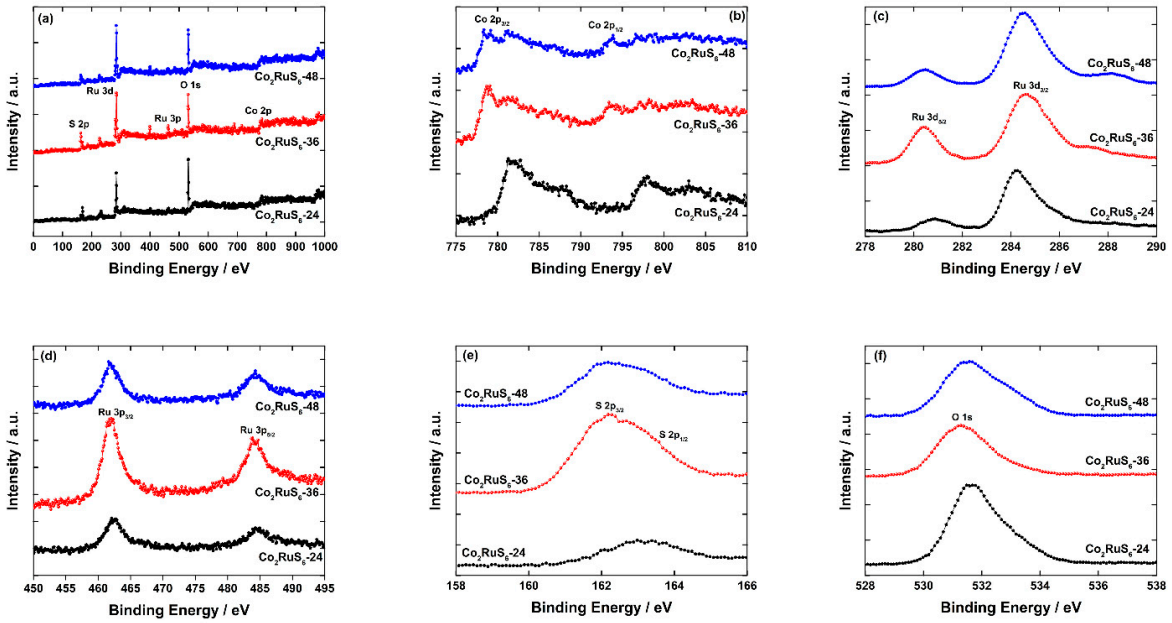

Figure 7. Typical XP spectra of the Co_2RuS_6-24, Co_2RuS_6-36, and Co_2RuS_6-48 samples: (**a**) survey spectra and (**b**) Co 2*p*, (**c**) Ru 3*d*, (**d**) Ru 3*p*, (**e**) S 2*p*, and (**f**) O 1*s* XP spectra.

As shown in Figure 7c, the deconvoluted spectrum of the Ru 3*d* state shows the presence of two peaks at 280.4 and 284.6 eV, corresponding to the divalent Ru $3d_{5/2}$ and Ru $3d_{3/2}$ states respectively. The difference between the two peaks (i.e., spin orbit splitting) is 4.2 eV [63]. As shown in Figure 7d, the deconvoluted spectrum of the Ru 3*p* state consists of two peaks centered at 461.9 eV and 484.4 eV, corresponding to the Ru $3p_{3/2}$ and Ru $3p_{1/2}$ states respectively [28,29]. The deconvoluted spectrum of sulfur states in cobalt ruthenium sulfide (Figure 7e) shows a main peak centered at 162.3 eV related

to the S $2p_{3/2}$ state. Figure 7f shows the presence of an XPS peak corresponding to O 1*s* at a binding energy of 531.3 eV. The above experimental results are in good agreement with previous XPS studies of metal sulfides, confirming the formation of ternary metal sulfides [28,29,49]. Based on the XPS analysis, the near-surface composition of the ternary sulfides is comprised of Co^{2+}/Co^{3+}, Ru^{2+}, and S^{2-}, which is characteristic of the Co_2RuS_6 phase.

Additionally, the XPS analyses suggest an atomic Co/Ru/S ratio of 1.87:0.91:4.96, which nearly matches stoichiometric Co_2RuS_6. These results are very similar to results obtained for ternary transition metal sulfides ($Co_{0.67}Fe_{0.33}S_2$), which are used as electrode materials for supercapacitor applications [49].

3.2. Electrochemical Performance

Metal sulfides are advanced materials for energy storage applications, such as supercapacitors and lithium-ion batteries. Many transition metal sulfides have attracted great attention as significant pseudocapacitive electrode materials for supercapacitors by virtue of their low electronegativity, good electrical conductivity, rich electrochemical redox sites, and large energy density. Still, their relatively low electrical conductivity and high volume changes severely hamper their use in wider commercial applications.

In this study, we analyzed the electrochemical behavior of all the cobalt ruthenium sulfides using CV (Figure 8a–d). The molar ratio of cobalt in the cobalt ruthenium sulfide microstructure enhances the electrochemical performance. The effect of the preparation time on the structure and electrochemical performance of cobalt ruthenium sulfide was studied. The specific capacitances (C_s) from cyclic voltammetric studies were calculated using the following formula:

$$C_s = (Q)(\Delta V \times m)^{-1} \quad (1)$$

where Q is the voltammetric charge, ΔV is the potential range, and m is the mass of the active material in the electrode. The C_s values of Co_2RuS_6-24 (50 F g^{-1}) and Co_2RuS_6-48 (70 F g^{-1}) are lower than that of Co_2RuS_6-36 (95 F g^{-1}) at a scan rate of 5 mV s^{-1} (Figure 8a). Furthermore, the cyclic voltammograms of the Co_2RuS_6-36 electrode material at different scan rates are demonstrated in Figure 8b. The shape of the cyclic voltammogram changes as the scan rate increases: the potentials of the anodic and cathodic peaks shift to slightly more positive and negative values, respectively, because of electrode polarization [64]. Figure 8c presents cyclic voltammograms of RuS_2, $CoRu_2S_6$, and $CoRuS_6$ electrode materials at a scan rate of 5 mV s^{-1}. $CoRu_2S_6$ and $CoRuS_6$ electrode samples showed similar cyclic voltammograms which both have lower integral areas than RuS_2 electrode thus showed less specific capacitances. The cyclic voltammograms of cobalt ruthenium sulfides feature a pair of redox peaks, indicating that the capacitance is governed by pseudocapacitance and electrochemical double layer capacitance. The specific capacitances of RuS_2 and cobalt ruthenium sulfides with different Co/Ru molar ratios and different time intervals are graphically represented in Figure 8d at a scan rate of 5 mV s^{-1}.

Figure 9a,b show typical GCD curves (2^{nd} cycles) for Co_2RuS_6-36 and Co_2RuS_6-24, respectively, at current densities of 1, 2, 3, and 5 A g^{-1} in a 0.5 M H_2SO_4 aqueous electrolyte within a potential range of 0–1 V (*vs.* Ag/AgCl). The specific capacitances (C_s) were calculated using the following formula:

$$C_s=(i\times\Delta t)\ (\Delta V\times m)^{-1} \quad (2)$$

where i is the applied constant current, Δt is the discharge time, ΔV is the potential range, and m is the mass of the electrode material. The symmetry of the charging and discharging characteristics at all current densities reflects the good capacitive behavior of all the electrode materials. The Co_2RuS_6-36 electrode material showed specific capacitances of 75, 64, 56, and 48 F g^{-1} at current densities of 1, 2, 3, and 5 A g^{-1}, respectively (Figure 9a). The specific capacitance of Co2RuS6 electrode material is superior to reported ruthenium oxide materials like bulk RuO_2 (49 F g^{-1}) [65] and porous RuO_2

(50 F g^{-1}) [66] and comparatively lower cost. Our reported electrode material demonstrated higher electrochemical performance compared to similar other metal sulfides, such as MoS_2 (17.5 F g^{-1}) [67], CuS (62 F g^{-1}) [68], WS_2 (40 F g^{-1}) [69], and carbon based materials like thermally reduced graphene oxide (47 F g^{-1}) [70]. In addition, 64% of the capacitance was preserved when the GCD rate was increased from 1 to 5 A g^{-1}, suggesting good rate capability.

The Co_2RuS_6-24 electrode material showed specific capacitances of 55, 53, 45, and 44 F g^{-1} at current densities of 1, 2, 3, and 5 A g^{-1}, respectively (Figure 9b). In addition, 80% of the capacitance was preserved when the GCD rate was increased from 1 to 5 A g^{-1}, suggesting excellent rate capability. Figure 9c shows typical GCD curves (2nd cycle) for $CoRu_2S_6$ (30 F g^{-1}), $CoRuS_6$ (35 F g^{-1}), and Co_2RuS_6 (45 F g^{-1}) electrodes, ternary metal sulfides prepared under the same reaction conditions (i.e., a reaction time of 24 h) with different Co/Ru molar ratios at a current density of 3 A g^{-1}. We can state that electrochemical performances affected by cobalt and ruthenium molar ratios in ternary metal sulfides. But, how it affects is still unclear and needs more research investigations.

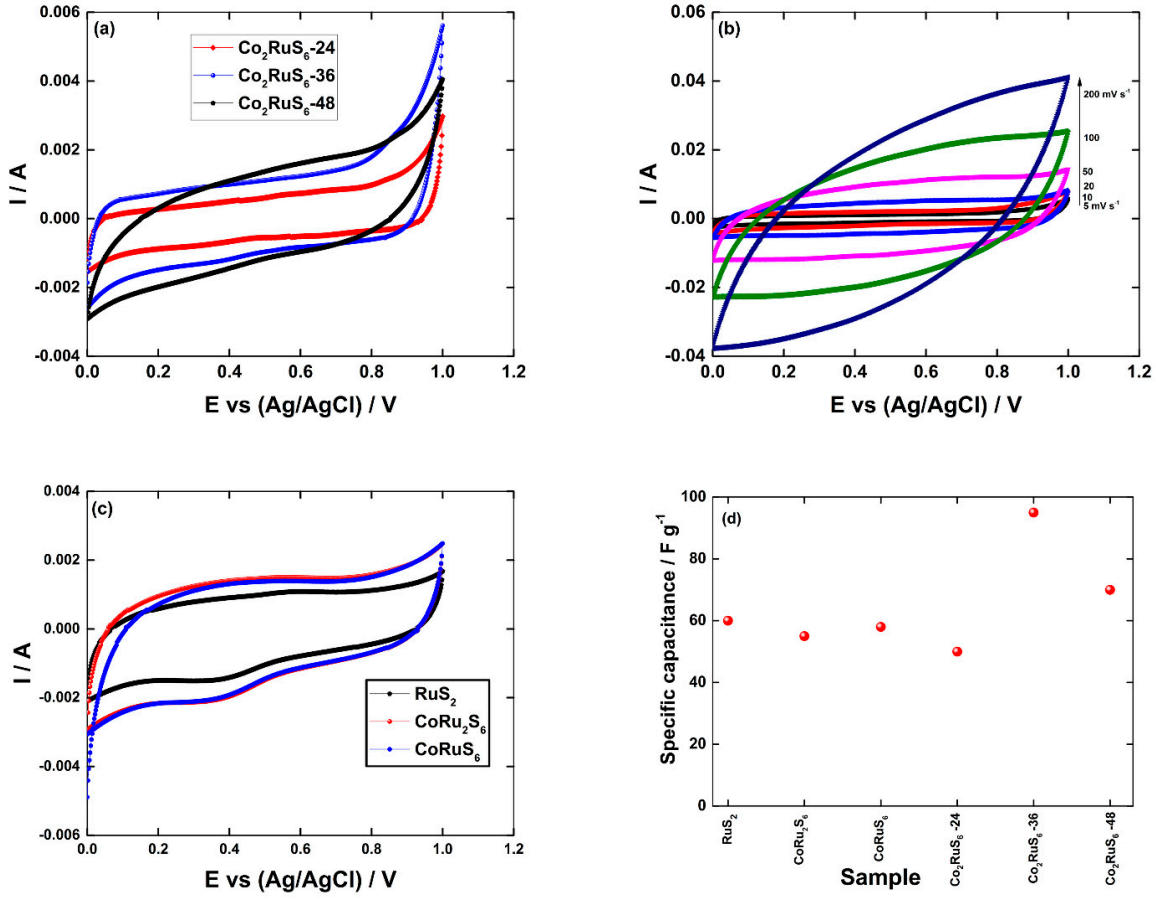

Figure 8. (**a**) Cyclic voltammograms of Co_2RuS_6-24, Co_2RuS_6-36, and Co_2RuS_6-48 electrode samples obtained at a scan rate of 5 mV s^{-1}. (**b**) Cyclic voltammograms of Co_2RuS_6-36 electrode sample obtained at scan rates of 5, 10, 20, 50, 100, and 200 mV s^{-1}. (**c**) Cyclic voltammograms of RuS_2, $CoRu_2S_6$, and $CoRuS_6$ electrode samples obtained at a scan rate of 5 mV s^{-1}. (**d**) Graphical representation of the specific capacitances of cobalt ruthenium sulfides with different molar ratios and different time intervals obtained at a scan rate of 5 mV s^{-1}.

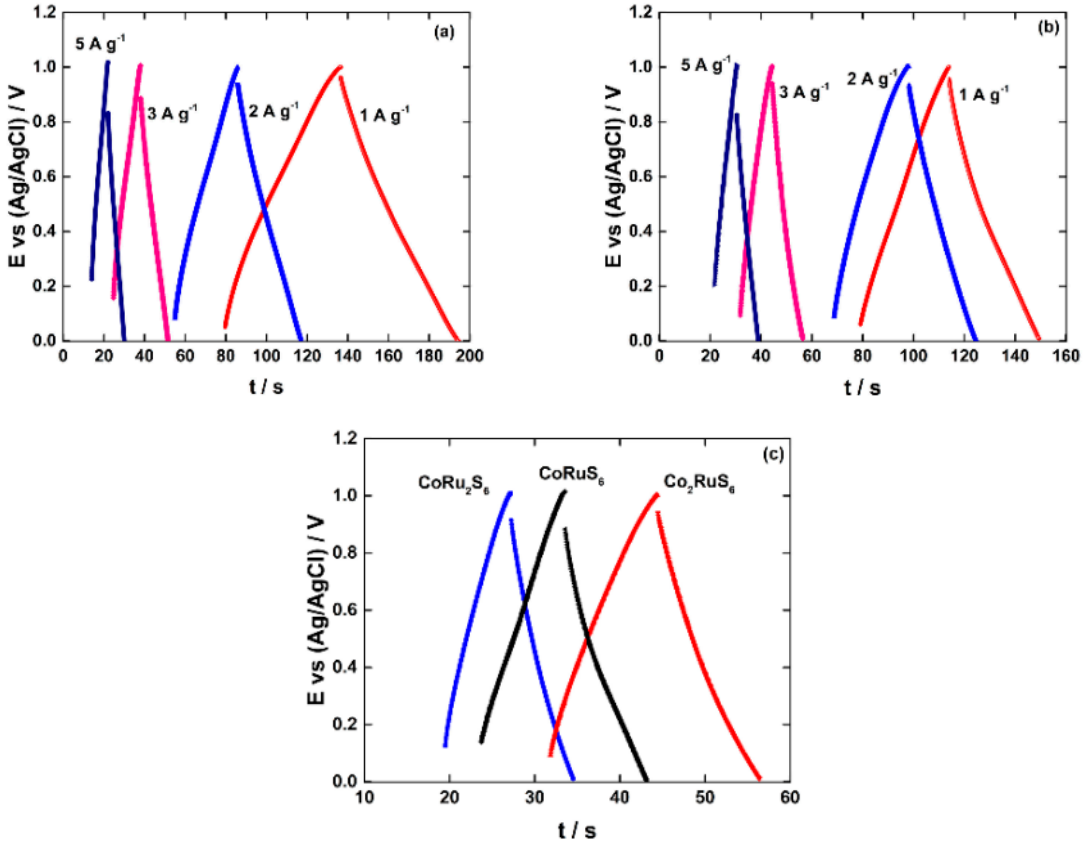

Figure 9. (**a**) GCD patterns of Co_2RuS_6-36 electrode samples at a variety of current densities. (**b**) GCD patterns of Co_2RuS_6-24 electrode samples at a variety of current densities. (**c**) GCD patterns of $CoRu_2S_6$, $CoRuS_6$, and Co_2RuS_6 electrode samples prepared at 24 h, with an applied current density of 3 A g^{-1}. (All GCD patterns of 2nd cycles are represented).

The gravimetric energy density (ED) and power density (PD) were calculated from the GCD measurements using the following formulas:

$$ED=0.5\times C\times(\Delta V)^2\times(3600)^{-1} \quad (3)$$

$$PD=ED/(\Delta t) \quad (4)$$

where C is the specific capacitance from charge/discharge studies, ΔV is the potential window, and Δt is the discharge time in charge/discharge cycles. The capacitance is constant, but the polarization limits the rate at which the charge may be delivered. This is an entirely kinetic phenomenon and not a thermodynamic one. The Co_2RuS_6-36 electrode material for supercapacitors showed an energy density of 10.5 Wh kg^{-1} and power density of 600 W kg^{-1} at a current density of 1 A g^{-1}. As the current density was increased from 1 to 5 A g^{-1}, the Co_2RuS_6-36 electrode material demonstrated an energy density of 6.7 Wh kg^{-1} and power density of 3001.5 W kg^{-1}. The Co_2RuS_6-24 composite electrode material for supercapacitors showed an energy density of 7.6 Wh kg^{-1} and power density of 600 W kg^{-1} at a current density of 1 A g^{-1}. As the current density was increased from 1 to 5 A g^{-1}, the Co_2RuS_6-24 electrode material exhibited an energy density of 6.1 Wh kg^{-1} and power density of 2745 W kg^{-1}.

Cycle stability is a critical characteristic for practical applications in energy storage devices. Figure 10 shows the cycling performance of the Co_2RuS_6-36 electrode material at a scan rate of 10 mV s^{-1}. Significantly, the electrode exhibited good electrochemical stability with 81% retention of its specific capacitance over 1000 cycles.

To further elucidate the electrode kinetics, diffusion behavior, and the electrochemical characteristics of the frequency response behavior of the cobalt ruthenium sulfides, electrochemical

impedance spectra were obtained in a frequency range of 100 KHz–0.1 Hz in the 0.5 M H_2SO_4 aqueous electrolyte. The results are shown in Figure 11 as Nyquist and Bode plots obtained at the open circuit voltage. The Nyquist plots comprise a semicircle in the high-frequency region, which originates from the charge-transfer resistance (R_{ct}), and a vertical line in the low-frequency region (Figure 11a). They reveal the pseudocapacitive behavior and porous structure of the electrode materials. The maximum phase angle was found to be approximately 68° (Figure 11b). The response frequency of the Co_2RuS_6-36 electrode supercapacitor measured at the open circuit voltage was 1.84 Hz, and the corresponding response time was 0.54 s. The electrolyte solution resistance (R_s) values for the Co_2RuS_6-24, Co_2RuS_6-36, and Co_2RuS_6-48 samples were 2.72 Ω, 2.4 Ω, and 1.65 Ω, respectively. The charge-transfer resistance (R_{ct}) values for the Co_2RuS_6-24, Co_2RuS_6-36, and Co_2RuS_6-48 electrode samples were 1.4, 0.9, and 3.15 Ω, respectively. This faradaic charge transfer resistance is closely associated with electron transfer at the electrode–electrolyte interface. The value of the charge transfer resistance (R_{ct}) is the main part of the resistance of the supercapacitor. If the materials show lower charge transfer resistance, this indicates higher electrical conductivity (i.e., fast response ability of the electrode) [64,71]. Very low values of R_s and R_{ct} indicate a fast charge-discharge process. All the Nyquist plots demonstrate Warburg impedance resistance behavior, which is associated with frequency-dependent ion-diffusion kinetics.

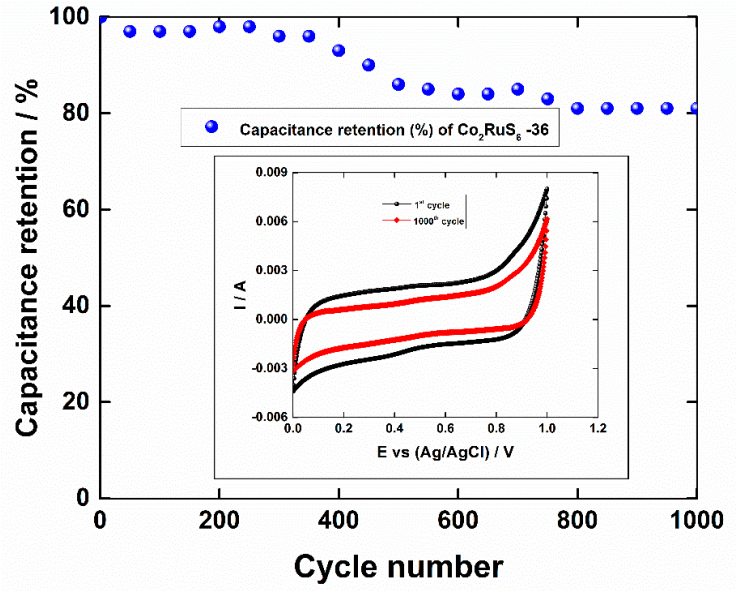

Figure 10. Cyclic stability performance of cyclic voltammetric cycles of Co_2RuS_6-36 electrode at a scan rate of 10 mV s^{-1}.

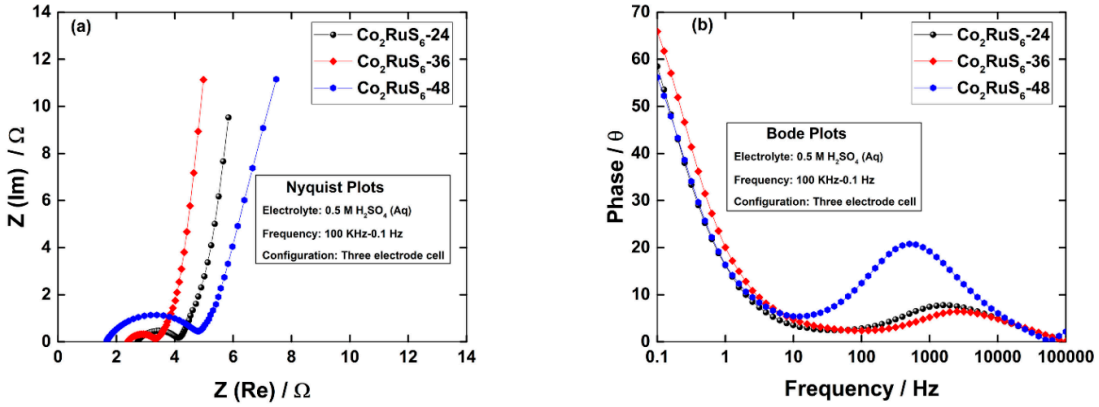

Figure 11. (**a**) Nyquist plots and (**b**) Bode plots of Co_2RuS_6-24, Co_2RuS_6-36, and Co_2RuS_6-48 electrode materials in the frequency range of 100 kHz–0.1 Hz in aqueous 0.5 M H_2SO_4 electrolyte.

4. Conclusions

In summary, we have successfully synthesized cobalt ruthenium sulfides through a facile, simple hydrothermal method. Ternary metal sulfides normally possess richer redox-active sites and the formation of cobalt ruthenium sulfides with the synergistic effect of the Co and Ru elements, which have multiple valence states, promotes ions diffusion on the surface of the electrode. This results in improved electrochemical activity and specific capacitance. All the prepared cobalt ruthenium sulfides showed nanocrystal morphology. Therefore, the Co_2RuS_6-36 electrode material for pseudocapacitors manifested a favorable specific capacitance of 75 F g^{-1} at 1 A g^{-1} along with an energy density of 10.5 Wh kg^{-1}, a power density of 600 W kg^{-1}, and a good cycling stability with 81% capacitance maintained after 1000 cycles, making this material a promising candidate for energy storage. This facile synthetic process represents an efficient way to prepare electrode materials with enhanced electrochemical properties.

Author Contributions: Conceptualization, R.B. and S.U.; Formal analysis, R.B. and S.U.; Funding acquisition, S.U.; Investigation, R.B.; Methodology, R.B.; Project administration, S.U.; Writing—original draft, R.B.; Writing—review & editing, S.U. All authors have read and agreed to the published version of the manuscript.

Funding: This work was supported by the Korea Evaluation Institute of Industrial Technology [grant No. 201900000002949] and the research fund of Hanyang University [grant No. 201700000002241].

Conflicts of Interest: The authors declare no conflict of interest.

References

1. Lin, T.; Chen, I.W.; Liu, F.; Yang, C.; Bi, H.; Xu, F.; Huang, F. Nitrogen-doped mesoporous carbon of extraordinary capacitance for electrochemical energy storage. *Science* **2015**, *350*, 1508–1513. [CrossRef]
2. Gonzalez, A.; Goikolea, E.; Barrena, J.A.; Mysyk, R. Review on supercapacitors: Technologies and materials. *Renew. Sust. Energ. Rev.* **2016**, *58*, 1189–1206. [CrossRef]
3. Wang, Y.; Song, Y.; Xia, Y. Electrochemical capacitors: mechanism, materials, systems, characterization and applications. *Chem. Soc. Rev.* **2016**, *45*, 5925–5950. [CrossRef] [PubMed]
4. Liu, C.; Li, F.; Ma, L.P.; Cheng, H.M. Advanced materials for energy storage. *Adv. Mater.* **2010**, *22*, E28–E62. [CrossRef] [PubMed]
5. Sahoo, M.K.; Rao, G.R. Fabrication of $NiCo_2S_4$ nanoball embedded nitrogen doped mesoporous carbon on nickel foam as an advanced charge storage material. *Electrochim. Acta* **2018**, *268*, 139–149. [CrossRef]
6. Lu, Y.; Li, B.; Zheng, S.; Xu, Y.; Xue, H.; Pang, H. Syntheses and energy storage applications of M_xS_y(M= Cu, Ag, Au) and their composites: rechargeable batteries and supercapacitors. *Adv. Funct. Mater.* **2017**, *27*, 1703949. [CrossRef]
7. Zhang, L.L.; Zhao, X.S. Carbon-based materials as supercapacitor electrodes. *Chem. Soc. Rev.* **2009**, *38*, 2520–2531. [CrossRef]
8. Wang, G.; Zhang, L.; Zhang, J. A review of electrode materials for electrochemical supercapacitors. *Chem. Soc. Rev.* **2012**, *41*, 797–828. [CrossRef]
9. Yuan, C.; Wu, H.B.; Xie, Y.; Lou, X.W. Mixed transition-metal oxides: design, synthesis, and energy-related applications. *Angew. Chem. Int. Ed.* **2014**, *53*, 1488–1504. [CrossRef]
10. Cottineau, T.; Toupin, M.; Delahaye, T.; Brousse, T.; Belanger, D. Nanostructured transition metal oxides for aqueous hybrid electrochemical supercapacitors. *Appl. Phys. A.* **2006**, *82*, 599–606. [CrossRef]
11. Deng, W.; Ji, X.; Chen, Q.; Banks, C.E. Electrochemical capacitors utilising transition metal oxides: an update of recent developments. *Rsc Adv.* **2011**, *1*, 1171–1178. [CrossRef]
12. Lokhande, C.D.; Dubal, D.P.; Joo, O.S. Metal oxide thin film based supercapacitors. *Curr. Appl. Phys.* **2011**, *11*, 255–270. [CrossRef]
13. Snook, G.A.; Kao, P.; Best, A.S. Conducting-polymer-based supercapacitor devices and electrodes. *J. Power Sources* **2011**, *196*, 1–12. [CrossRef]
14. Bolagam, R.; Boddula, R.; Srinivasan, P. Synthesis of highly crystalline polyaniline with the use of (Cyclohexylamino)-1-propanesulfonic acid for supercapacitor. *J. Appl. Electrochem.* **2015**, *45*, 51–56. [CrossRef]

15. Rajender, B.; Palaniappan, S. Organic solvent soluble methyltriphenylphosphonium peroxodisulfate: a novel oxidant for the synthesis of polyaniline and the thus prepared polyaniline in high performance supercapacitors. *New J. Chem.* **2015**, *39*, 5382–5388. [CrossRef]
16. Jiang, J.; Li, Y.; Liu, J.; Huang, X.; Yuan, C.; Lou, X.W. Recent advances in metal oxide-based electrode architecture design for electrochemical energy storage. *Adv. Mater.* **2012**, *24*, 5166–5180. [CrossRef]
17. Augustyn, V.; Simon, P.; Dunn, B. Pseudocapacitive oxide materials for high-rate electrochemical energy storage. *Energy Environ. Sci.* **2014**, *7*, 1597–1614. [CrossRef]
18. Inagaki, M.; Konno, H.; Tanaike, O. Carbon materials for electrochemical capacitors. *J. Power Sources* **2010**, *195*, 7880–7903. [CrossRef]
19. Bolagam, R.; Boddula, R.; Srinivasan, P. One-step preparation of sulfonated carbon and subsequent preparation of hybrid material with polyaniline salt: a promising supercapacitor electrode material. *J. Solid State Electrochem.* **2017**, *21*, 1313–1322. [CrossRef]
20. Eftekhari, A.; Li, L.; Yang, Y. Polyaniline supercapacitors. *J. Power Sources* **2017**, *347*, 86–107. [CrossRef]
21. Bolagam, R.; Srinivasan, P. Use of oil in the polymerization of aniline to polyaniline salt containing dual dopants, sulfuric acid, and castor oil: material for high-performance supercapacitor. *Ionics* **2017**, *23*, 1277–1284. [CrossRef]
22. Yu, X.Y.; Lou, X.W. Mixed metal sulfides for electrochemical energy storage and conversion. *Adv. Energy Mater.* **2018**, *8*, 1701592. [CrossRef]
23. Sahoo, S.; Pazhamalai, P.; Krishnamoorthy, K.; Kim, S.J. Hydrothermally prepared α-MnSe nanoparticles as a new pseudocapacitive electrode material for supercapacitor. *Electrochim. Acta* **2018**, *268*, 403–410. [CrossRef]
24. Chhowalla, M.; Shin, H.S.; Eda, G.; Li, L.J.; Loh, K.P.; Zhang, H. The chemistry of two-dimensional layered transition metal dichalcogenide nanosheets. *Nat. Chem.* **2013**, *5*, 263–275. [CrossRef] [PubMed]
25. Yu, X.Y.; Yu, L.; Lou, X.W.D. Metal sulfide hollow nanostructures for electrochemical energy storage. *Adv. Energy Mater.* **2016**, *6*, 1501333. [CrossRef]
26. Rui, X.; Tan, H.; Yan, Q. Nanostructured metal sulfides for energy storage. *Nanoscale* **2014**, *6*, 9889–9924. [CrossRef] [PubMed]
27. Yu, X.Y.; Yu, L.; Shen, L.; Song, X.; Chen, H.; Lou, X.W.D. General formation of MS (M= Ni, Cu, Mn) box-in-box hollow structures with enhanced pseudocapacitive properties. *Adv. Funct. Mater.* **2014**, *24*, 7440–7446. [CrossRef]
28. Krishnamoorthy, K.; Pazhamalai, P.; Kim, S.J. Ruthenium sulfide nanoparticles as a new pseudocapacitive material for supercapacitor. *Electrochim. Acta* **2017**, *227*, 85–94. [CrossRef]
29. Bolagam, R.; Um, S. L-cysteine-assisted synthesis of ruthenium sulfide/thermally reduced graphene oxide nanocomposites: Promising electrode materials for high-performance energy storage applications. *Electrochim. Acta* **2018**, *281*, 571–581. [CrossRef]
30. Patil, S.J.; Kim, J.H.; Lee, D.W. Graphene-nanosheet wrapped cobalt sulphide as a binder free hybrid electrode for asymmetric solid-state supercapacitor. *J. Power Sources* **2017**, *342*, 652–665. [CrossRef]
31. Luo, F.; Li, J.; Yuan, H.; Xiao, D. Rapid synthesis of three-dimensional flower-like cobalt sulfide hierarchitectures by microwave assisted heating method for high-performance supercapacitors. *Electrochim. Acta* **2014**, *123*, 183–189. [CrossRef]
32. Guo, Y.; Zhang, W.; Sun, Y.; Dai, M. Ruthenium nanoparticles stabilized by mercaptan and acetylene derivatives with supercapacitor application. *Electrochim. Acta* **2018**, *270*, 284–293. [CrossRef]
33. Dubal, D.P.; Gund, G.S.; Holze, R.; Jadhav, H.S.; Lokhande, C.D.; Park, C.J. Solution-based binder-free synthetic approach of RuO_2 thin films for all solid state supercapacitors. *Electrochim. Acta* **2015**, *103*, 103–109. [CrossRef]
34. Kulkarni, P.; Nataraj, S.K.; Balakrishna, R.G.; Nagaraju, D.H.; Reddy, M.V. Nanostructured binary and ternary metal sulfides: synthesis methods and their application in energy conversion and storage devices. *J. Mater. Chem. A.* **2017**, *5*, 22040–22094. [CrossRef]
35. Dubal, D.P.; Chodankar, N.R.; Holze, R.; Kim, D.H.; Gomez-Romero, P. Ultrathin Mesoporous $RuCo_2O_4$ Nanoflakes: An Advanced Electrode for High-Performance Asymmetric Supercapacitors. *Chem. Sus. Chem.* **2017**, *10*, 1771–1782. [CrossRef]
36. Shen, L.; Wang, J.; Xu, G.; Li, H.; Dou, H.; Zhang, X. $NiCo_2S_4$ nanosheets grown on nitrogen-doped carbon foams as an advanced electrode for supercapacitors. *Adv. Energy Mater.* **2015**, *5*, 1400977. [CrossRef]

37. Guo, S.; Chen, W.; Li, M.; Wang, J.; Liu, F.; Cheng, J.P. Effect of reaction temperature on the amorphous-crystalline transition of copper cobalt sulfide for supercapacitors. *Electrochim. Acta* **2018**, *271*, 498–506. [CrossRef]
38. Xu, X.; Liu, W.; Kim, Y.; Cho, J. Nanostructured transition metal sulfides for lithium ion batteries: Progress and challenges. *Nano Today* **2014**, *9*, 604–630. [CrossRef]
39. Gulen, M.; Sarilmaz, A.; Patir, I.H.; Ozel, F.; Sonmezoglu, S. Ternary copper-tungsten-disulfide nanocube inks as catalyst for highly efficient dye-sensitized solar cells. *Electrochim. Acta* **2018**, *269*, 119–127. [CrossRef]
40. Geng, P.; Zheng, S.; Tang, H.; Zhu, R.; Zhang, L.; Cao, S.; Xue, H.; Pang, H. Transition metal sulfides based on graphene for electrochemical energy storage. *Adv. Energy Mater.* **2018**, *8*, 1703259. [CrossRef]
41. Jiang, Y.; Qian, X.; Zhu, X.; Liu, H.; Hou, L. Nickel cobalt sulfide double-shelled hollow nanospheres as superior bifunctional electrocatalysts for photovoltaics and alkaline hydrogen evolution. *Acs Appl. Mater. Interfaces* **2018**, *10*, 9379–9389. [CrossRef] [PubMed]
42. Liu, Y.; Li, Y.; Kang, H.; Jin, T.; Jiao, L. Design, synthesis, and energy-related applications of metal sulfides. *Mater. Horiz.* **2016**, *3*, 402–421. [CrossRef]
43. Deng, C.; Yang, L.; Yang, C.; Shen, P.; Zhao, L.; Wang, Z.; Wang, C.; Li, J.; Qian, D. Spinel $FeCo_2S_4$ nanoflower arrays grown on Ni foam as novel binder-free electrodes for long-cycle-life supercapacitors. *Appl. Surf. Sci.* **2018**, *428*, 148–153. [CrossRef]
44. Rajesh, J.A.; Park, J.H.; Quy, V.H.V.; Kwon, J.M.; Chae, J.; Kang, S.H.; Kim, H.; Ahn, K.S. Rambutan-like cobalt nickel sulfide ($CoNi_2S_4$) hierarchitecture for high-performance symmetric aqueous supercapacitors. *J. Ind. Eng. Chem.* **2018**, *63*, 73–83. [CrossRef]
45. Liu, S.; Jun, S.C. Hierarchical manganese cobalt sulfide core–shell nanostructures for high-performance asymmetric supercapacitors. *J. Power Sources* **2017**, *342*, 629–637. [CrossRef]
46. Gao, Y.P.; Huang, K.J. $NiCo_2S_4$ materials for supercapacitor applications. *Chem. Asian J.* **2017**, *12*, 1969–1984. [CrossRef]
47. Li, B.; Zheng, M.; Xue, H.; Pang, H. High performance electrochemical capacitor materials focusing on nickel based materials. *Inorg. Chem. Front.* **2016**, *3*, 175–202. [CrossRef]
48. Huang, T.; Song, X.Z.; Chen, X.; Chen, X.L.; Sun, F.F.; Su, Q.F.; Li, L.D.; Tan, Z. Carbon coated nickel–cobalt bimetallic sulfides hollow dodecahedrons for a supercapacitor with enhanced electrochemical performance. *New J. Chem.* **2018**, *42*, 5128–5134. [CrossRef]
49. Liu, W.; Niu, H.; Yang, J.; Cheng, K.; Ye, K.; Zhu, K.; Wang, G.; Cao, D.; Yan, J. Ternary transition metal sulfides embedded in graphene nanosheets as both the anode and cathode for high-performance asymmetric supercapacitors. *Chem. Mater.* **2018**, *30*, 1055–1068. [CrossRef]
50. Guan, B.Y.; Yu, L.; Wang, X.; Song, S.; Lou, X.W. Formation of onion-like $NiCo_2S_4$ particles via sequential ion-exchange for hybrid supercapacitors. *Adv. Mater.* **2017**, *29*, 1605051. [CrossRef]
51. Kristl, M.; Dojer, B.; Gyergyek, S.; Kristl, J. Synthesis of nickel and cobalt sulfide nanoparticles using a low cost sonochemical method. *Heliyon* **2017**, *3*, e00273. [CrossRef] [PubMed]
52. Lin, Y.; Yu, J.; Xing, Z.; Guo, X.; Yu, X.; Tang, B.; Zou, J. Enhanced generation of H_2O_2 and radicals on Co_9S_8/partly-graphitized carbon cathode for degradation of bio-refractory organic wastewater. *Electrochim. Acta* **2016**, *213*, 341–350. [CrossRef]
53. Wang, Z.; Pan, L.; Hu, H.; Zhao, S. Co_9S_8 nanotubes synthesized on the basis of nanoscale Kirkendall effect and their magnetic and electrochemical properties. *Cryst. Eng. Comm.* **2010**, *12*, 1899–1904. [CrossRef]
54. Tang, X.; Huang, J.; Feng, Q.; Liu, K.; Luo, X.; Li, Z. Carbon sphere@Co_9S_8 yolk-shell structure with good morphology stability for improved lithium storage performance. *Nanotechnology* **2017**, *28*, 375402. [CrossRef] [PubMed]
55. Meng, X.; Deng, J.; Zhu, J.; Bi, J.; Kan, E.; Wang, X. Cobalt sulfide/graphene composite hydrogel as electrode for high-performance pseudocapacitors. *Sci. Rep.* **2016**, *6*, 21717. [CrossRef] [PubMed]
56. Wang, H.; Lu, S.; Chen, Y.; Han, L.; Zhou, J.; Wu, X.; Qin, W. Graphene/Co_9S_8 nanocomposite paper as a binder-free and free-standing anode for lithium-ion batteries. *J. Mater. Chem. A.* **2015**, *3*, 23677–23683. [CrossRef]
57. Xie, S.; Deng, Y.; Mei, J.; Yang, Z.; Lau, W.M.; Liu, H. Facile synthesis of CoS_2/CNTs composite and its exploitation in thermal battery fabrication. *Composites Part. B.* **2016**, *93*, 203–209. [CrossRef]
58. Cai, X.; Shen, X.; Ma, L.; Ji, Z. Facile synthesis of nickel–cobalt sulfide/reduced graphene oxide hybrid with enhanced capacitive performance. *Rsc Adv.* **2015**, *5*, 58777–58783. [CrossRef]

59. Li, Y.; Li, N.; Yanagisawa, K.; Li, X.; Yan, X. Hydrothermal synthesis of highly crystalline RuS_2 nanoparticles as cathodic catalysts in the methanol fuel cell and hydrochloric acid electrolysis. *Mater. Res. Bull.* **2015**, *65*, 110–115. [CrossRef]
60. Gabold, H.; Luan, Z.; Paul, N.; Opel, M.; Müller-Buschbaum, P.; Law, M.; Paul, A. Structural and magnetic properties of cobalt iron disulfide ($Co_xFe_{1-x}S_2$) nanocrystals. *Sci. Rep.* **2018**, *8*, 4835. [CrossRef]
61. Li, M.L.; Xiao, K.; Su, J.; Li, N.; Cai, Y.P.; Liu, Z.Q. $CuCo_2S_4$ nanosheets coupled with carbon nanotube heterostructures for highly efficient capacitive energy storage. *Chem. Electro. Chem.* **2018**, *5*, 2496–2502.
62. Xiao, J.; Wan, L.; Yang, S.; Xiao, F.; Wang, S. Design hierarchical electrodes with highly conductive $NiCo_2S_4$ nanotube arrays grown on carbon fiber paper for high-performance pseudocapacitors. *Nano Lett.* **2014**, *14*, 831–838. [CrossRef] [PubMed]
63. Jeevanandam, P.; Koltypin, Y.; Gofer, Y.; Diamant, Y.; Gedanken, A. Sonochemical synthesis of nanocrystallites of ruthenium sulfide, $RuS_{1.7}$. *J. Mater. Chem.* **2000**, *10*, 2769–2773. [CrossRef]
64. Singu, B.S.; Yoon, K.R. Synthesis and characterization of MnO_2-decorated graphene for supercapacitors. *Electrochim. Acta* **2017**, *231*, 749–758. [CrossRef]
65. Hu, C.-C.; Huang, Y.-H.; Chang, K.-H. Annealing effects on the physicochemical characteristics of hydrous ruthenium and ruthenium–iridium oxides for electrochemical supercapacitors. *J. Power Sources* **2002**, *108*, 117–127. [CrossRef]
66. Patake, V.D.; Lokhande, C.D. Chemical synthesis of nano-porous ruthenium oxide (RuO_2) thin films for supercapacitor application. *App. Surf. Sci.* **2008**, *254*, 2820–2824. [CrossRef]
67. Krishnamoorthy, K.; Pazhamalai, P.; Veerasubramani, G.K.; Kim, S.-J. Mechanically delaminated few layered MoS_2 nanosheets based high performance wire type solid-state symmetric supercapacitors. *J. Power Sources.* **2016**, *321*, 112–119. [CrossRef]
68. Krishnamoorthy, K.; Veerasubramani, G.K.; Radhakrishnan, S.; Kim, S.-J. Preparation of copper sulfide nanoparticles by sonochemical method and study on their electrochemical properties. *J. Nanosci. Nanotechnol.* **2015**, *15*, 4409–4413. [CrossRef]
69. Mayorga-Martinez, C.C.; Ambrosi, A.; Eng, A.Y.S.; Sofer, Z.; Pumera, M. Transition metal dichalcogenides (MoS_2, $MoSe_2$, WS_2 and WSe_2) exfoliation technique has strong influence upon their capacitance. *Electrochem. Commun.* **2015**, *56*, 24–28. [CrossRef]
70. Chen, C.M.; Zhang, Q.; Yang, M.G.; Huang, C.H.; Yang, Y.G.; Wang, M.Z. Structural evolution during annealing of thermally reduced graphene nanosheets for application in supercapacitors. *Carbon* **2012**, *50*, 3572–3584. [CrossRef]
71. Bolagam, R.; Boddula, R.; Srinivasan, P. Hybrid material of PANI with TiO_2-SnO_2: Pseudocapacitor electrode for higher performance supercapacitors. *Chem. Sel.* **2017**, *2*, 65–73. [CrossRef]